Numerical Investigation into the Pressure and Flow Velocity Distributions of a Slender-Body Catamaran Due to Viscous Interference Effects

I Ketut Aria Pria Utama[1,2*], Wasis Dwi Aryawan[1], Ahmad Nasirudin[1,3], Sutiyo[4], Yanuar[5]

[1]Department of Naval Architecture, Institute of Technology Sepuluh Nopember, Surabaya 60111, Indonesia
[2]Research Center for Marine-Earth Science and Technology, Institute of Technology Sepuluh Nopember, Surabaya 6011, Indonesia
[3]Department of Systems and Naval Mechatronic Engineering, National Cheng Kung University, Tainan 710, Taiwan
[4]Department of Naval Architecture, University of Hang Tuah, Surabaya 60111, Indonesia
[5]Department of Mechanical Engineering, Faculty of Engineering, Universitas Indonesia, Kampus UI Depok, Depok 16424, Indonesia

Abstract. A computational fluid dynamics investigation was carried out on a slender body catamaran to determine the effect of pressure and flow velocity changes for varied hull separations. The investigation was conducted using an NPL 4a model with a slenderness (length to breadth) ratio of about 11 together with the use of a commercial code (CFX) with hull separations of $S/L = 0.3$ and 0.4 along with a variation in Reynolds numbers of 2.86×10^5, 3.43×10^5, 4.01×10^5, and 4.44×10^5. Pressure and flow velocity around the hull were measured to obtain a fluid effect attributed to the influence of catamaran hull interference. A computational fluid dynamics investigation was carried out with the same configurations as those in the experimental tests. The overall results were in good agreement, with the order of discrepancy at about 1.76%; the computational fluid dynamics results were consistently lower than the experimental ones. Both tests demonstrated a viscous interaction between the hulls and, thus, the form factors for the demihull and catamaran were properly derived: the form factor for the demihull $(1+k)$ was 1.254 and for the catamaran $(1+\beta k)$ was 1.420, indicating interaction effects of about 13.2%. The form factor for the catamaran was consistently higher than the demihull, suggesting some viscous interference between the hulls. The effect of catamaran hull interference variation can be recognized through the velocity augmentation ratio (σ), pressure change ratio (ϕ), and the viscous interference factor (β). In addition, the β value is very helpful for finding out the interference of the hull on a catamaran when sophisticated experimental and numerical tools are not available.

Keywords: Catamaran; CFD; Flow velocity; Pressure distribution; Viscous interference factor

1. Introduction

Multihull ships have progressively received considerable attention. One of the most popular is the catamaran (Utama, 1999). Catamarans have a unique hydrodynamics phenomenon known as viscous and wave interactions which occur between the demihull of the catamaran. The technique to conduct and analyze the viscous resistance of a catamaran can be done using the computational fluid dynamics (CFD) method on a reflex model. In this case, the free surface is treated, allowing the isolation of the viscous

resistance by omitting any influences from surface waves. The use of reflex models in a CFD simulation, therefore, provides an approximate means of directly measuring the total viscous resistance of the model without wave resistance.

In the last 50 years, the development of catamaran theory has been proposed by many researchers to explain the resistance of catamarans. The reflex model was a technique pioneered by Joubert and Matheson (1970), where the resistance of the hull was measured in a wind tunnel. Utama (1999) conducted a detailed experimental investigation in a low-speed wind tunnel on a single ellipsoid (as a reflex model) and a pair of ellipsoids nearby representing a catamaran. Theoretical, numerical, and experimental investigations have been carried out on multihull vessels and further research has been conducted by Zaghi et al. (2011).

An increasing number of researchers are calculating ship resistance using CFD. Broglia et al. (2014) completed a study on catamarans with Froude numbers between 0.3 and 0.5 which showed that the configuration of the narrow hull distance between catamarans has a more significant interference effect. Numerical computation to illustrate the hydrodynamic factors that influence ship resistance using a FLUENT code has been investigated by Deng et al. (2011). Jamaluddin et al. (2013) conducted experimental and numerical investigations to analyze the components of resistance and interactions between hulls in catamarans, and Samuel et al. (2015) studied the selection of optimal catamaran hulls on traditional fishing vessels.

Previous studies have discussed a lot of catamaran hull interference, but not many have conducted detailed research related to interference due to viscous form factors. Broglia et al. (2019) have been conducting research to improve the capabilities of state-of-the-art CFD tools in the prediction of the flow-field around a multihull catamaran. Viscous resistance represents an integral part of the total resistance of a catamaran in which intermediate Froude Number value interference effects are dominant (Farkas et al., 2017). A potential-flow method was carried out to determine the lift force of single-deadrise hulls and catamaran configurations in which hydrodynamics pressure was more pronounced between two catamaran hulls (Bari and Matveev, 2017). Iqbal and Samuel, (2017) have conducted research catamaran hull form show that the fluid form that surrounds the ship hull influences ship resistance. Mittendorf and Papanikolaou (2020) investigated catamaran resistance and also found an increase in total resistance due to viscous interference. Therefore, the CFD technique could be used to optimize the hull of a catamaran (Miao et al., 2020; Yongxing and Kim, 2020).

The study objectives were to determine the viscous interference due to pressure and flow velocity changes between the catamaran hulls by using a reflex model and to derive viscous form factors (β) in the catamaran models using CFD. The results were validated with an experimental investigation which was carried out in a wind tunnel on a symmetrical catamaran using a reflex model of NPL4a by Jamaluddin et al. (2013).

2.   Methods

2.1. Model Description

This investigation used the NPL4a model, as shown in the body-plan form in Figure 1. The priority of the study was to investigate how viscous interference effects are affected by hull form; thus, the NPL4a model was fully cut lengthwise at the draft, as shown in Figure 1a. The model is also reflected lengthwise, as shown in Figure 1b. Using reflex model that is immersed in water causes the effect of waves on the model to disappear. The principal particulars of the model are given in Table 1.
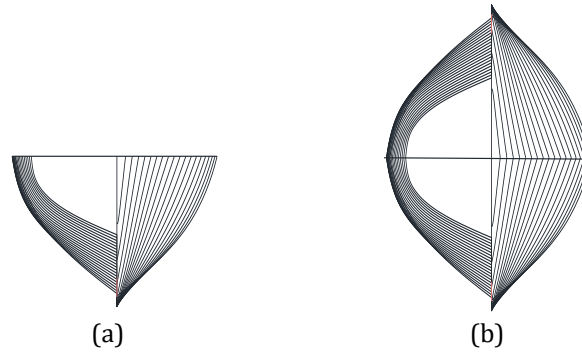
(a)   (b)

Figure 1 NPL4a model: (a) model at the draft; (b) reflex model

Table 1 Principal particulars of the model

Parameter	Dimension	Demihull	Unit
Length	L_{WL}	0.457	m
Breadth	B	0.410	m
Draft	T	0.260	m
Separation ratio 0.3	S/L = 0.3	0.137	m
Separation ratio 0.4	S/L = 0.4	0.187	m
Wetted surface area	WSA	0.284	m^2
Volume	V	5.332×10^{-2}	m^3
Displacement	Δ	0.534	kg
Block coefficient	Cb	0.397	
Prismatic coefficient	Cp	0.769	

2.2. Mathematical Model

The Reynolds-averaged Navier–Stokes (RANS) method is a three-dimensional equation that was developed and used in the CFD model. One of the equations was developed by ANSYS, Inc. is CFX software which unsteady viscous incompressible flow to solve flow problems in the walls of ships. For instance, a flow field is characterized by a balance in mass, momentum, and total energy described by the continuity equation (Ferziger et al., 1997). The equations of mass and momentum can be written as shown in Equations 1 and 2.

$$\frac{\partial \rho}{\partial t} + \nabla.(\rho U) = 0$$

(1)

$$\frac{\partial(\rho U)}{\partial t} + \nabla.(\rho UU) = -\nabla p + \nabla.\tau + S_M$$

(2)

where the stress tensor, τ, is related to the strain rate, as shown in Equation 3:

$$\tau = \mu\left(\nabla U + (\nabla U)^T\right) - \frac{2}{3}\delta\nabla.U$$

(3)

The term $+\nabla(U.\tau)$ represents the work due to viscous stresses and is called the viscous work term. The term $U.S_M$ represents the work due to external momentum sources and is currently neglected.

Furthermore, the RANS method was introduced which was configured by modifying the unsteady Navier–Stokes by involving averaged and fluctuating quantities. The turbulence model based on the RANS equation is, according to (Anderson, 1995), a statistical turbulence model caused by the procedure of statistical average used to obtain the equations. Reynolds' average equations are given in Equations 4 and 5:

$$\frac{\partial \rho}{\partial t} + \frac{\partial}{\partial x_j}\left(\rho U_j\right) = 0 \tag{4}$$

$$\frac{\partial \rho}{\partial t} + \frac{\partial}{\partial x_j}\left(\rho U_i U_j\right) = -\frac{\partial p}{\partial x_j} + \frac{\partial}{\partial x_j}\left(\tau_{ij} - \overline{\rho u_i u_j}\right) + S_M \tag{5}$$

where τ is the stress tensor molecular consisting of normal and shear stress components.

2.3. SST Turbulence Model

The Sheer Stress Transport turbulence model combines the advantages of the k-ω model to achieve an optimal model formulation for a wide range of applications. For this, a blending function, F1, is introduced which is equal to 1 near the solid surface and equal to 0 for the flow domain away from the wall. It activates the k-ω wall region and the k-ε model for the rest of the flow. Using this approach, the attractive near-wall performance of the k-ω model can be used without potential errors resulting from the free stream sensitivity of that model. The modelled equations for the turbulent kinetic energy k and the turbulence frequency ω are as follows:

$$\frac{\partial(\rho k)}{\partial t} + \frac{\partial(\partial u_j k)}{\partial x_j} = P - \beta * \rho \omega k + \frac{\partial}{\partial x_j}\left[\left(\mu + \sigma_k \mu_t\right)\frac{\partial k}{\partial x_j}\right] \tag{6}$$

$$\frac{\partial(\rho \omega)}{\partial t} + \frac{\partial(\partial u_j \omega)}{\partial x_j} = \frac{\gamma}{v_t} P - \beta \rho \omega^2 + \frac{\partial}{\partial x_j}\left[\left(\mu + \sigma_\omega \mu_t\right)\frac{\partial \omega}{\partial x_j}\right] + 2(1 - F_1)2\rho_{\omega 2}\frac{1}{\omega}\frac{\partial k}{\partial x_j}\frac{\partial \omega}{\partial x_j} \tag{7}$$

The performance of the SST turbulence model has been reported by Menter and Esch (2001). In a NASA technical memorandum by Bardina et al. (1997), the SST model was rated the most accurate model in its class.

2.4. Numerical Modelling

The main objective of this CFD study was to investigate the effect of viscous interference due to the interaction of two ship hulls. Transversal (S/L) distance variations were applied. The CFD technique with the current setup investigated the air flow pressure by assuming that the grid independence study was carried out for a catamaran. The grid-sensitivity study on the application of the International Towing Tank Conference (2002) uncertainty was performed by simulating four different grids and assuming a sufficient ratio to obtain a grid-independent solution for each model.

2.4.1. Computational domain

This research applied a single-phase fluid flow simulation together with the use of an ANSYS CFX commercial code. The most recommended computational domain at the velocity inlet was set at 1.5L forward perpendicular to the front and at the outlet pressure was 3.5L towards the back which was measured perpendicularly. To eliminate the effect of backward viscous pressure on the side boundaries, the transverse and vertical directions were set at 1.5L (Elkafas et al., 2019), as shown in Figure 2. The downstream boundary condition was determined as pressure outflow by adjusting the static pressure to prevent reverse flow (Ford and Winroth, 2019).

(a)
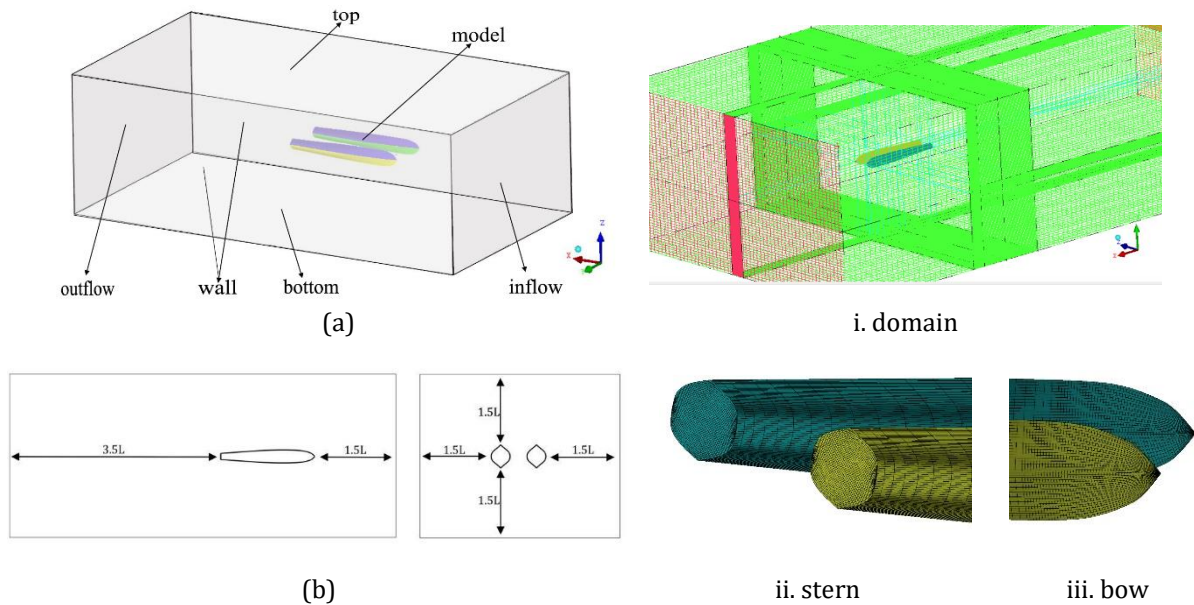
i. domain

(b)

ii. stern   iii. bow

Figure 2 Numerical modelling: (a) boundary condition; (b) computational domain; (c) structured mesh model

2.4.2. Mesh generation

The application of a structured mesh in any aspect of the grid generation has certain advantages. One special case on the clever use of a structured mesh is the adoption of block-structured or multiblock meshes. Through this approach, the mesh of the domain in question is now assembled from several structured blocks that are attached to one another (Tu et al., 2018). This type of mesh layer allows the CFD to be able to accurately complete the flow near the wall of the model by describing the flow separation near the hull (ANSYS, 2020). The number of mesh layers were chosen correctly to meet the number of y+ of less than 1 on the wall near the ship (ITTC, 2014), as shown in Figure 3.
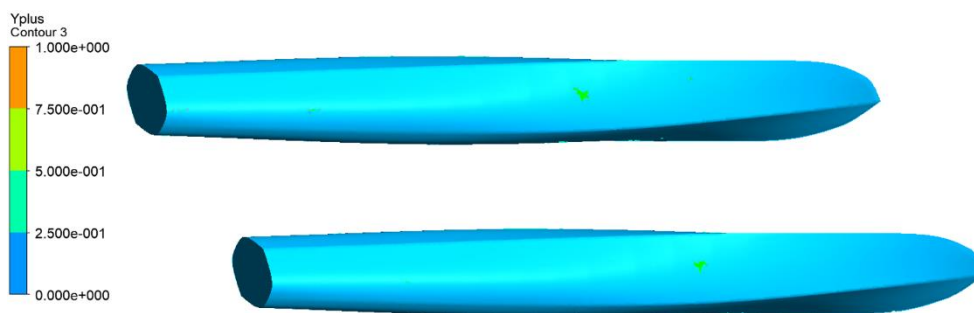

Figure 3 Wall y+ distribution on the hull surface

2.4.3. Convergence and grid independence

An essential aspect of the calculation of numerical simulation is the convergence and history records that describe the working time of a variable amplitude deviation comprehensive approach to the CFD simulation. The root-mean-square (RMS) criteria used to check the convergence with a residual target value (variable value) reaching 10^{-5} and the results are shown in Figure 4a. These residual monitors demonstrate monotonic convergence, indicating a well-posed problem and a tightly converged solution (ANSYS, 2020).

The large number of cells or grids used in the calculation will determine the accuracy of the results. The number of cells affects the change in geometric shape at the time of processing the results. The selection of the number of meshing through the independence study approach grid is shown in Figure 4b. A simulation of grid independence was performed on catamaran reflex models with S/L = 0.4 at Re = 4.44×10^5 with air media. Grid independence studies showed that optimal catamaran reflex model simulations on grid number 1,352,075 with have a viscous resistance coefficient of 8.661×10^{-3} resistance to optimal difference C_V of 0.44%.
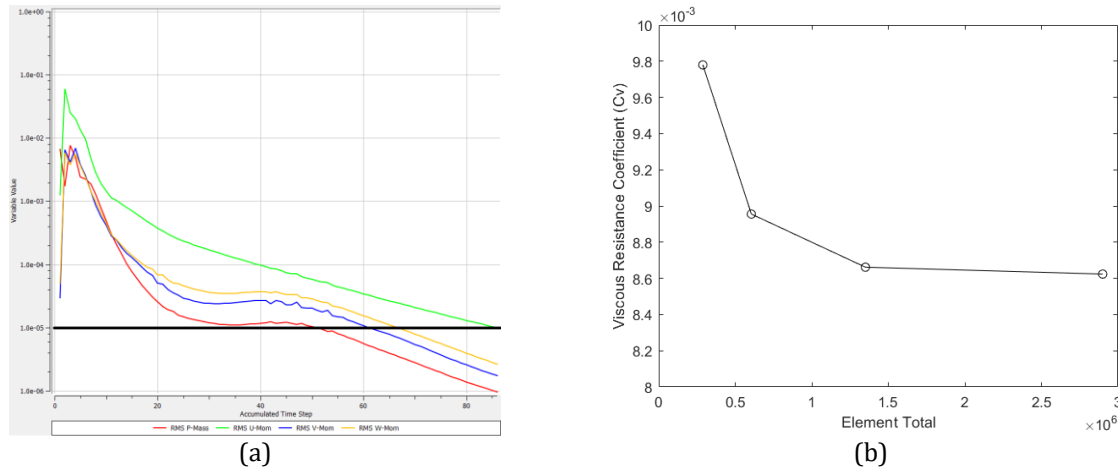

| (a) | (b) |

Figure 4 (a) Convergency; (b) grid independence study

2.5. Placement of Pressure Tappings on Physical Model and Points on CFD Simulation

The physical model testing in the wind tunnel was focused on calculating the viscous resistance and changes in pressure and flow velocity between the two catamaran hulls. In the wind tunnel simulation, the model was assumed to be stationary and the fluid (wind) to be moving at a specified speed. The airflow in the wind tunnel test section must move homogeneously laterally, longitudinally, and vertically, both in terms of speed, static pressure, angularity, and turbulence intensity.

The location of the front test model (in the test section of the wind tunnel) faces the direction of the flow. Then the pressure and velocity of flow between the hulls can be properly measured. The pressure on the hull model surface (consisting of 44 pressure taps) is used to determine the pressure distribution around the hull. Longitudinal and circumferential positions of the pressure tappings are shown in Figure 5a (Jamaluddin et al., 2013). Each pressure tap on the hull is connected to a manometer tube or pressure transducer (a flow and pressure measuring instrument) in the order specified. The data obtained from the measuring instrument was processed into a pressure coefficient which was then used to calculate the pressure on the surface of the model test object (hull).

The CFD simulation was set to test the wind tunnel by determining the points on the surface of the ship model that function the same as the pressure tappings in the wind tunnel testing, as shown in Figure 5b. The placement of pressure tappings in the experimental model and points in the simulation model serve to calculate the pressure at those locations.
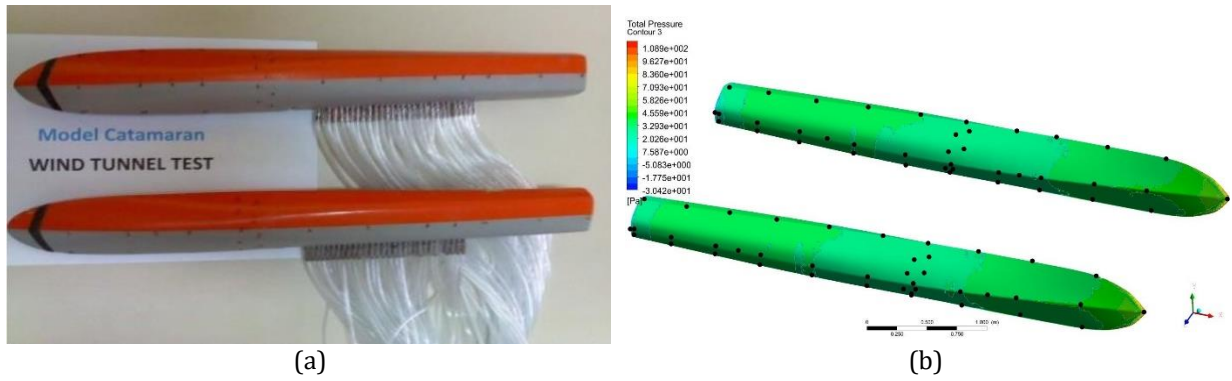
(a) (b)

Figure 5 (a) Placement pressure tapping in the experiment model; (b) placement points on the simulation model
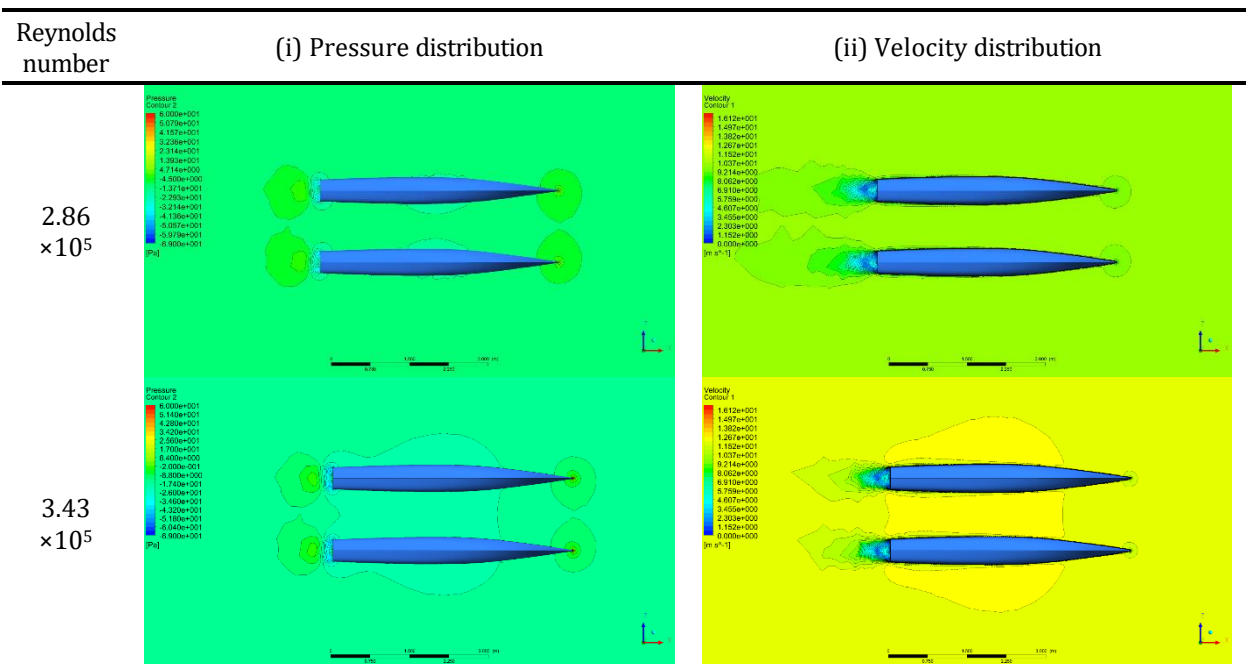
3. Results and Discussion

3.1. Pressure and Velocity Characteristics

The catamaran reflex model has unique flow velocity and pressure characteristics in the hull: the flow inside will interact between the two hulls, while the outside will interact with one hull. This will cause a difference in velocity and pressure between the inside and outside of the catamaran hull.

3.1.1. Ratio of separation to length, S/L = 0.3

There is a change in inner hull pressure at Re = 2.86×10^5 to 4.44×10^5 which is quite clear. The pressure interaction of the inner hull occurs at Re = 3.43×10^5 to 4.44×10^5. In general, the pressure interaction of the inner hull is smaller than that of the outer hull. This also occurs in the flow distribution, where there is an interaction at Re = 2.86×10^5 to 4.44×10^5, and a significant interaction of the inner hull flow occurs at Re = 4.44×10^5. This is explained in detail in Figure 6: changes in low flow velocity occur around the bow of the ship and then increase to the stern hull. This phenomenon occurs because the fluid flow on the hull occurs freely and is not influenced by the other hull.
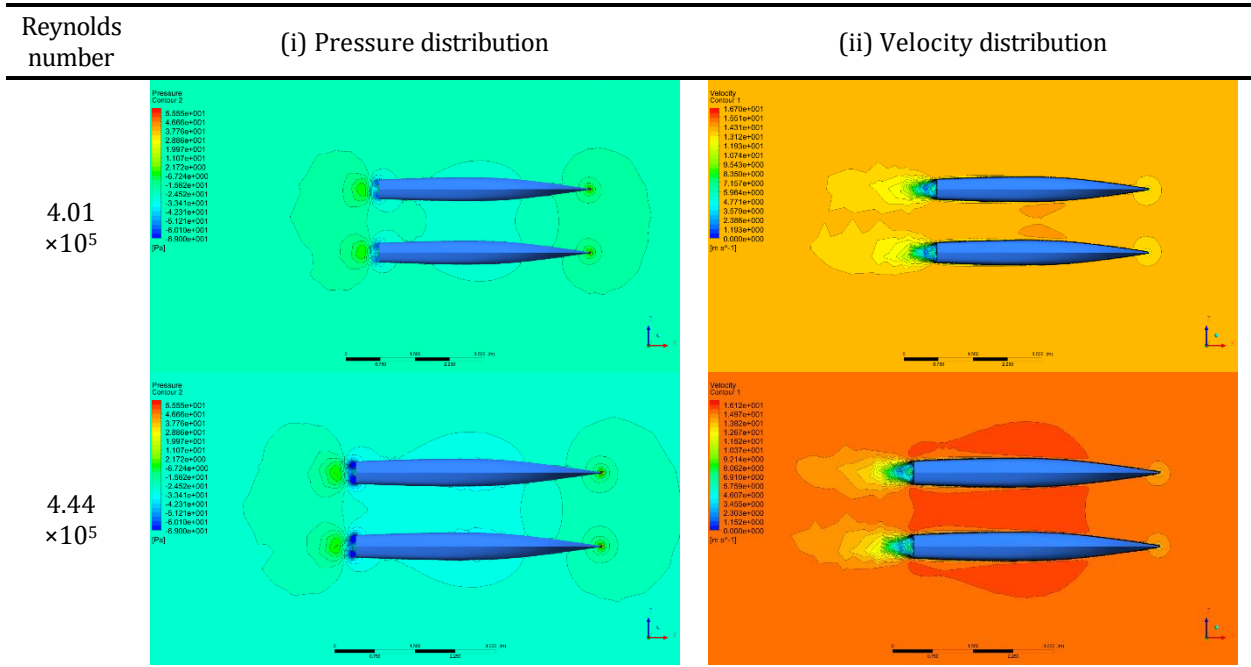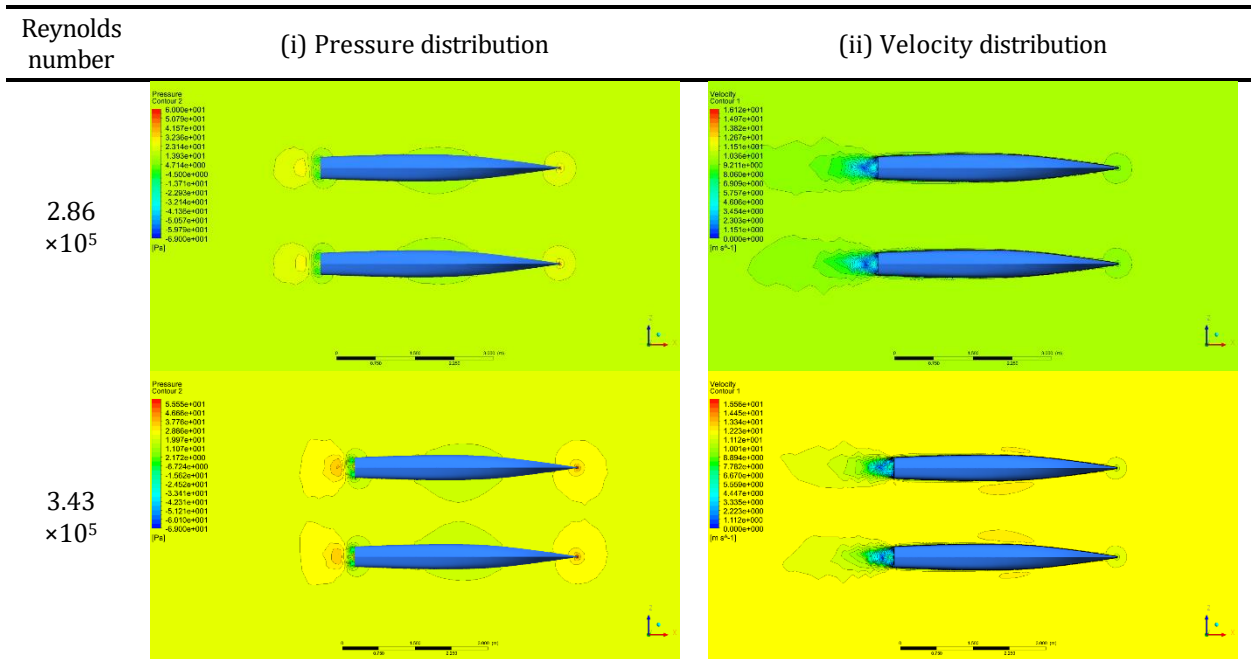
Reynolds number	(i) Pressure distribution	(ii) Velocity distribution
2.86 ×10⁵		
3.43 ×10⁵		

Reynolds number	(i) Pressure distribution	(ii) Velocity distribution
4.01 ×10⁵		
4.44 ×10⁵		

Figure 6 Pressure and velocity distribution for the catamaran (S/L = 0.3)

3.1.2. Ratio of separation to length, S/L = 0.4

The change in inner hull pressure at Re = $2.86×10^5$ to $4.44×10^5$ is quite clear. Likewise, the inner hull velocity distribution has quite a clear difference. This phenomenon shows that the flow velocity has a significant influence on the inner hull pressure and flow due to the interaction between the hulls, as shown in Figure 7.
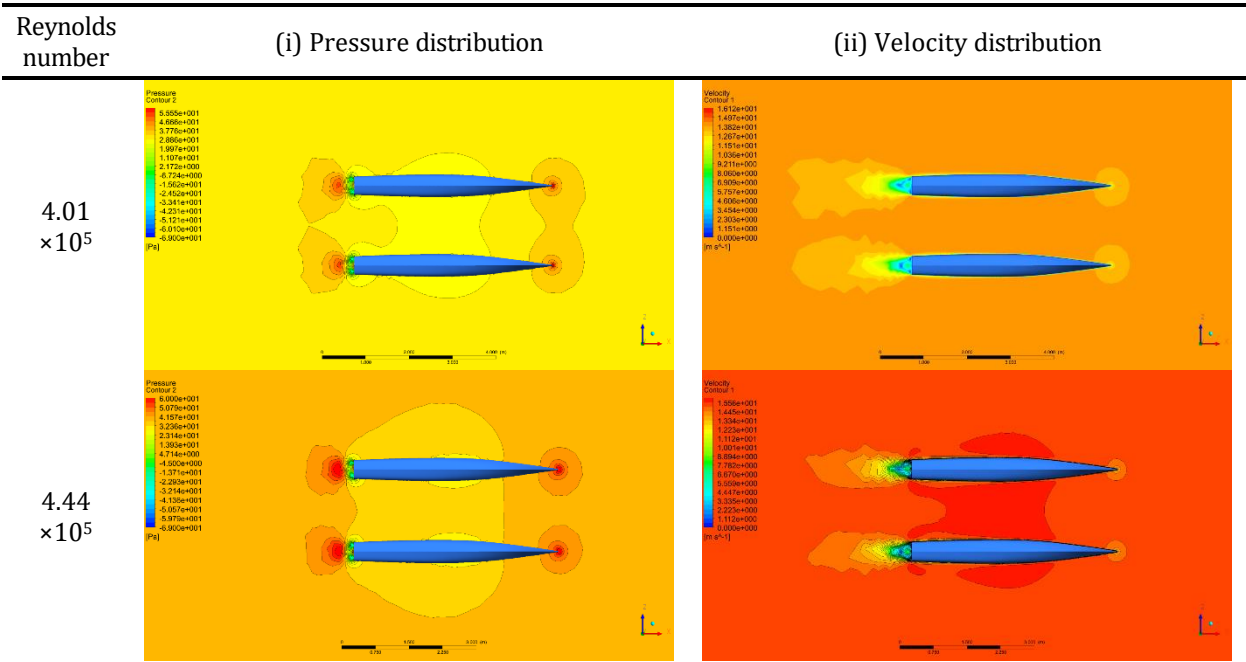
Reynolds number	(i) Pressure distribution	(ii) Velocity distribution
2.86 ×10⁵		
3.43 ×10⁵		

Reynolds number	(i) Pressure distribution	(ii) Velocity distribution
4.01 ×10⁵		
4.44 ×10⁵		

Figure 7 Pressure and velocity distribution for the catamaran; S/L = 0.4

3.2. Comparison with Experiment

A comparison between the CFD results and the experimental work was made with the work done by Jamaluddin et al. (2013). In this case, two parameters were analyzed, namely the flow velocity augmentation ratio (σ) and the pressure change ratio (ϕ). The speed ratio consistently shows a value of more than 1, meaning that the velocity in the inner hull is greater than that of the outer hull. This is caused by narrowing the waterway bordered by the two hulls of the catamaran. The pressure has a value less than 1, which means that the inner hull pressure is smaller than the outer hull because of the higher velocity between the hulls of the catamaran than the outer hull, as shown in Figures 8.

Differences occur in the experiment and the numerical model which could be due to surface roughness. The experimental model has a higher level of roughness than the numerical model, so the calculation results in the experiment are greater.
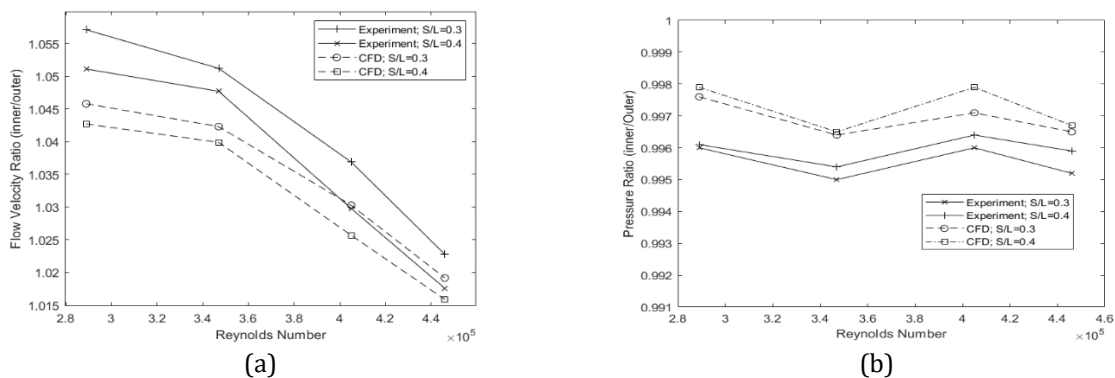

(a)　　　　　　　　　　(b)

Figure 8 (a) Ratio of flow velocity changes based on Re and S/L; (b) ratio of pressure changes based on Re and S/L

Furthermore, Insel and Molland (1992) defined the viscous resistance of catamaran hulls, as shown in Equation 10.

$$\left(C_v\right)_{CAT} = \left(1 + \phi k\right)\sigma C_F$$

(10)

The friction resistance for the experiment was determined using the ITTC-57 extrapolation line (ITTC, 2002), as shown in Equation 11:

$$C_F = \frac{0.075}{\left(\log Re - 2\right)^2}$$

(11)

where Re is the Reynolds number.

The C_F for the CFD simulation is obtained from the formula, as follows:

$$C_F = \frac{\tau}{0.5\rho v^2}$$

(12)

where τ is the wall shear, ρ is density of air ($\rho = 1.225$ kg/m³), and v is velocity of air in m/s.

The viscous resistance on the hull consists of pressure drag and friction drag or shear force. Frictional resistance is the drag force due to the viscosity of the fluid tangent to the surface of the hull and pressure resistance is a normal force due to fluid pressure around the hulls.

Pressure resistance may be estimated by integrating pressure coefficients over the hull (Utama, 1999; Armstrong, 2003; Molland et al., 2017), as written in Equation 13.

$$C_{VP} = \int C_P ds$$

(13)

where C_P is the pressure coefficient, C_{VP} is the viscous pressure resistance coefficient, and ds is the distance between two pressure coefficients.

Disturbed flow velocity around the hull (demihull) increases in the inner area (between the hull), hence it changes the structure of the boundary layer and the area of the side of the hull. Changes in the physical structure of the boundary layer and the area of the side of the hull cause friction resistance (skin friction) increases or decreases which can then change the value of the form factor.

Since C_{VP} (Equation 13) is based on the maximum cross-sectional area (CSA), and C'_{VP} is based on the wetted surface area (WSA), the results must be multiplied by a factor (CSA/WSA). Further information on the conversion can be found in Utama (1999). The corrected C'_{VP} is then:

$$C'_{VP} = \frac{CSA}{WSA} C_{VP}$$

(14)

where CSA = 7.778×10⁻³ m² and WSA = 0.284 m². Calculation of the viscous resistance coefficient (C_V) is a summation of viscous pressure resistance (C'_{VP}) and Coefficient friction (C_F). The results obtained for the viscous pressure resistance coefficient (C'_{VP}) and viscous resistance coefficient (C_V) are shown in Figures 9a and 9b, respectively.

In addition, it is also seen that the value of C_P affects the velocity (Re), and the trend of the C_P curve follows the same pattern for several variations of distance between the tubes (S/L). The greater the speed, the greater the pressure coefficient value on the hull.

The numerical simulation and the experiment (wind tunnel) showed that the differences in the value of the component resistance are relatively small (an average of 1.76%) and both models have a viscous form factor that shows a very accurate consistency. These calculation results were similar to those carried out by Jamaluddin et al. (2013). The viscous drag of the catamaran has an average of 13.2% greater than that of the demihull and this was caused by the viscous interaction between the hulls. The results obtained from these calculations are also in line with research by Yanuar et al., (2020) which the graph trend of the total drag coefficient (C_T) to the variation of the clearance distance (S/L) decreased along with the increase in clearance (S/L).
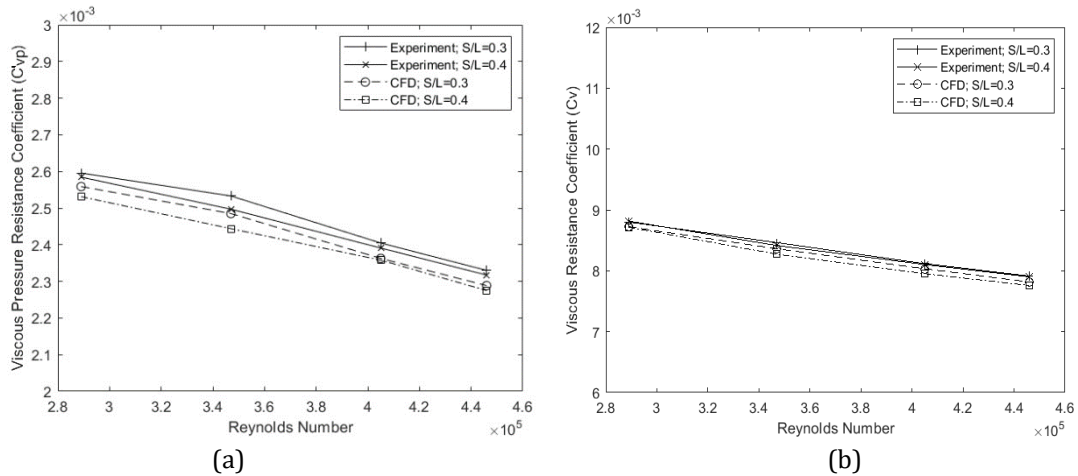
Figure 9 (a) Viscous pressure resistance coefficient; (b) viscous resistance coefficient

The value of the interference factor of the resistance component for the catamaran hull to the variation in the change in the distance between the hulls (S/L) is calculated based on the equation below.

$$IF_V = \frac{C_{VCAT}}{C_{VDEMI}} = \frac{\left[(1+\phi k)\sigma C_F\right]_{CAT}}{\left[(1+k)C_F\right]_{DEMI}}$$

(15)

where C_{VCAT} is the viscous resistance coefficient for the catamaran hulls and C_{VDEMI} for the demihulls.

Table 2 shows the viscous resistance interference for the variation in distance between the hulls (S/L) based on the viscous resistance value from the experimental results in the wind tunnel and the CFD.

Table 2 Viscous resistance interference factor

| Hull configuration | Re | Viscous interference | |
		Expt.	CFD
S/L = 0.3	2.89×10^5	1.10763	1.10763
	3.47×10^5	1.10759	1.10798
	4.05×10^5	1.10786	1.10802
	4.46×10^5	1.10792	1.10865
S/L = 0.4	2.89×10^5	1.10371	1.10458
	3.47×10^5	1.10375	1.10536
	4.05×10^5	1.10381	1.10569
	4.46×10^5	1.10386	1.10568

The phenomenon of the interaction of viscous interference is caused by the distribution of boundary layer changes and the increase in flow velocity around the catamaran hull, and the distribution of the effect of pressure changes in the area (between) the two hulls.

Determining the interference effect in the past was difficult, as separating ϕ and σ required the availability of high-performance computing and experimental tools (Insel and Molland, 1992). For practical purposes, ϕ and σ are combined into a viscous interference factor (β), where:

$$(1+\phi k)\sigma = (1+\beta)k$$

(16)

Then,

$$\beta = \frac{FF_{Cat} - 1}{FF_{Demi} - 1}$$

(17)

where FF_{Demi} is the form factor of the Demihull = 1+k and FF_{Cat} is the form factor of the catamaran = 1+βk.

The viscous interference factors (β) are shown in Table 3. The viscous interference factor (β) shows that the average form factors obtained from the CFD code have the same trend as the experiment's S/L increases, where for S/L = 0.3 they are higher than S/L = 0.4. The demihull form factor (1+k) has a smaller value than the catamaran form factor (1+βk) due to hull interference, which has an average of 13.2%. This has also been investigated by Molland et al. (1996). The form factor has quite a large influence on the viscous interference factor, β.

Table 3 Viscous form factor values

Method	Demihull (1+k)	Catamaran			
		1+βk		β	
		S/L = 0.3	S/L = 0.4	S/L = 0.3	S/L = 0.4
Experiment	1.265	1.415	1.410	1.566	1.547
CFD	1.257	1.391	1.382	1.521	1.486

4.   Conclusions

The effects of two variations of hull separations for a catamaran, which were investigated by CFD analysis, were compared with a wind tunnel experiment to validate the results. Numerical simulation and experiment (wind tunnel) results show a relatively small difference in the value of flow and pressure components, which is 1.76% on average. This result shows consistency and is entirely accurate. The difference in viscous resistance is about 13.2%, where the catamaran resistance is greater than that of the demihull and is attributed to the interaction between the hulls of the catamaran. The numerical simulation clearly illustrates the change in flow at the inner hulls which causes the result that viscous resistance at S/L = 0.3 is higher than that at S/L = 0.4. Also, it applies to the pressure acting on the model catamaran; the viscous pressure increases as the S/L decreases. The effect of the catamaran hull interference variation can be recognized through the velocity augmentation ratio (σ), pressure change ratio (φ), and viscous interference factor (β). The influence of interference resistance between two ship hulls causes the symmetrical flow of water around the demihull to be asymmetrical due to high pressure (which relates to σ) and flow velocity (associated with φ) which occurs around the hull and is relatively unequal to the hull centerline. In addition, the β value is very helpful for finding out the hull interference on a catamaran when sophisticated experimental and numerical tools are not available.

Acknowledgements

References

Anderson, J.D., 1995. *Computational Fluid Dynamics: The Basics with Applications, Editions:*

Mechanical Engineering. McGraw-Hill, New York, USA. pp. 526–532

ANSYS, 2020. *ANSYS CFX-Solver Theory Guide*. Ansys Inc, Canonsburg, PA, USA.

Armstrong, T., 2003. The Effect of Demihull Separation on the Frictional Resistance of Catamarans, *In:* The 7th International Conference on Fast Sea Transportation (FAST), 7th-10th October 2003. Ischia, Italy

Bardina, J.E., Huang, P.G., Coakley, T.J., 1997. *Turbulence Modeling Validation, Testing, and Development*. Nasa Technical, Memorandum

Bari, G.S., Matveev, K.I., 2017. Hydrodynamics of Single-Deadrise Hulls and Their Catamaran Configurations. *International Journal of Naval Architecture and Ocean Engineering*, Volumw 9(3), pp. 305–314

Broglia, R., Jacob, B., Zaghi, S., Stern, F., Olivieri, A., 2014. Experimental Investigation of Interference Effects for High-Speed Catamarans. *Ocean Engineering,* Volume 76, pp. 75–85

Broglia, R., Zaghi, S., Campana, E.F., Dogan, T., Sadat-Hosseini, H., Stern, F., Queutey, P., Visonneau, M., Milanov, E., 2019. Assessment of Computational Fluid Dynamics Capabilities for the Prediction of Three-Dimensional Separated Flows: The Delft 372 Catamaran in Static Drift Conditions. *Journal of Fluids Engineering*, Volume 41(9), pp. 1–28

Deng, R., Huang, D.B., Yu, L., Cheng, X.K., Liang, H.G., 2011. Research on Factors of a Flow Fieldaffecting Catamaran Resistance Calculation. *Harbin Gongcheng Daxue Xuebao/Journal Harbin Engineering University*. Volume 32(2), pp. 141–147

Elkafas, A.G., Elgohary, M.M., Zeid, A.E., 2019. Numerical Study on the Hydrodynamic Drag Force of a Container Ship Model. *Alexandria Engineering Journal*, Volume 58(3), pp. 849–859

Farkas, A., Degiuli, N., Martić, I., 2017. Numerical Investigation into the Interaction of Resistance Components for a Series 60 Catamaran. *Ocean Engineering,* Volume 146, pp. 151–169

Ferziger, J.H., Peric, M., Leonard, A., 1997. *Computational Methods for Fluid Dynamics*. Phys. Today.

Ford, C.L., Winroth, P.M., 2019. On the Scaling and Topology of Confined Bluff-Body Flows. *Journal of Fluid Mechanic,* Volume 876, pp. 1018–1040

Insel, M., Molland, A.F., 1992. *An Investigation Into Resistance Components of High Speed Displacement Catamarans*. RINA. UK., Volume 134, pp. 1–20

Iqbal, M., Samuel, 2017. Traditional Catamaran Hull Form Configurations that Reduce Total Resistance. *International Journal of Technology*, Volume 8(1), pp. 85–93

ITTC, 2014. Practical Guidelines for Ship CFD Applications. *In:* ITTC – Recomm. Proceeding Guidel. ITTC 7.5–03 –02, 1-9. Denmark.

ITTC, 2002. ITTC – Recommended Procedures Testing and Extrapolation Methods Resistance Test. *In:* International Towing Tank Conference

Jamaluddin, A., Utama, I., Widodo, B., Molland, A., 2013. Experimental and Numerical Study of the Resistance Component Interactions of Catamarans. *In:* Proceedings of the Institution of Mechanical Engineers, Part M: Journal of Engineering for the Maritime Environment. Volume 227, pp. 51–60

Joubert, P.N., Matheson, N., 1970. Wind Tunnel Tests of Two Lucy Ashton Relfex Geosims. *Journal of Ship Research,* Volume 14(04), pp. 241–276

Menter, F.R., Esch, T., 2001. Elements of Industrial Heat Transfer Predictions. 16th Brazilian Congress of Mechanical Engineering , *Energy and Power Engineering*, Volume 9(13), pp. 829–842

Miao, A., Zhao, M., Wan, D., 2020. CFD-Based Multi-Objective Optimisation of S60 Catamaran

Considering Demihull Shape and Separation. *Applied Ocean Research*, Volume 97, doi.org/10.1016/j.apor.2020.102071

Mittendorf, M., Papanikolaou, A.D., 2020. Hydrodynamic Hull Form Optimization of Fast Catamarans using Surrogate Models. *Ship Technology Research,* Volume 68(1), doi.org/10.1080/09377255.2020.1802165

Molland, A.F., Turnock, S.R., Hudson, D.A., 2017. *Ship Resistance and Propulsion.* Practical Estimation of Ship Propulsive Power. Second Edition, Cambridge University Press

Molland, A.F., Wellicome, J.F., Couser, P.R., 1996. *Resistance Experiments on a Systematic Series of High Speed Catamaran Forms: Variation of Length-Displacement Ratio and Breadth-Draught Ratio*. Trans. RINA. UK.

Samuel, Iqbal, M., Utama, I.K.A.P., 2015. An Investigation into the Resistance Components of Converting a Traditional Monohull Fishing Vessel into Catamaran Form. *International Journal of Technology*, Volume 6(3), pp. 432–441

Tu, J., Yeoh, G.-H., Liu, C., 2018. Chapter 4-CFD Mesh Generation: A Practical Guideline, *in: Computational Fluid Dynamics.* Elsevier, UK, pp. 125–154

Utama, I.K.A., 1999. *Investigation of the Viscous Resistance Components of Catamaran Forms*. Dissertation. University of Southampton,UK.

Yanuar., Gunawan., Utomo, A.S.A., Luthfi, M.N., Baezal, M.A.B., Majid, F.R.S., Chairunisa, Z., 2020. Numerical and Experimental Analysis of Total Hull Resistance on Floating Catamaran Pontoon for N219 Seaplanes based on Biomimetics Design with Clearance Configuration. *International Journal of Technology*, Volume 11(7), pp. 1397–1405

Yongxing, Z., Kim, D.-J., 2020. Optimization Approach for a Catamaran Hull using CAESES and STAR-CCM+. *Journal of Ocean Engineering and Technology,* Volume 34(4), pp. 272–276

Zaghi, S., Broglia, R., Di Mascio, A., 2011. Analysis of the Interference Effects for High-Speed Catamarans by Model Tests and Numerical Simulations. *Ocean Engineering,* Volume 38(17-18), pp. 2110–2122